ISBN: 978-3-95450-233-2 ISSN: 2673-5504 doi:10.18429/JACoW-SRF2021-WEPCAV011

PRESENT STATUS OF THE SPOKE CAVITY PROTOTYPING FOR THE JAEA-ADS LINAC

J. Tamura*, Y. Kondo, F.M. Maekawa, S. Meigo, B. Yee-Rendon, JAEA, Ibaraki, Japan
T. Dohmae, E. Kako, H. Sakai, K. Umemori, KEK, Ibaraki, Japan

Abstract

The Japan Atomic Energy Agency (JAEA) is proposing an accelerator-driven subcritical system (ADS) for efficient reduction of high-level radioactive waste generated in nuclear power plants. One of the challenging R&Ds for ADS is the reliability of the accelerator. In preparation for the full-scale design of the proton linac for the JAEA-ADS, we are now prototyping a single-spoke cavity for low-beta (around 0.2) beam acceleration. As there is no experience of manufacturing a superconducting spoke cavity in Japan, the cavity prototyping and performance testing are essential to ensure the feasibility of the JAEA-ADS linac. To proceed to an actual cavity fabrication, we have carefully reviewed the fabrication process. And then, we examined the electron-beam welding using niobium test pieces and investigated the welding condition for realizing the smooth underbead. We have finally started the press forming of niobium sheets and the machine work to shape the cavity parts. Now, we are parparing for the electron-beam welding of the shaped niobium parts.

INTRODUCTION

The Japan Atomic Energy Agency (JAEA) is proposing an accelerator-driven subcritical system (ADS) as a future project to transmute long-lived nuclides to short-lived or stable ones. In the JAEA-ADS, a high-power (30 MW) proton beam with a final beam energy of 1.5 GeV is required with high reliability. Furthermore, the accelerator needs to be operated in a continuous-wave (CW) mode in order to be compatible with the reactor operation. Since a normal conducting (NC) structure raises a difficulty in cavity cooling under the CW operation, a superconducting (SC) linac would be a suitable solution. Figure 1 shows the accelerating structure proposed for the JAEA-ADS linac. In the proposed linac, the high-intensity proton beam is accelerated by an NC radio-frequency quadruple (RFQ) and low-beta SC cavities such as half-wave resonators (HWRs) and single-spoke resonators (SSRs), and accelerated to the final beam energy of 1.5 GeV by elliptical cavities (ELLs). This accelerating structure is similar to that proposed in [1], and the latest design of the JAEA-ADS linac is reported in [2].

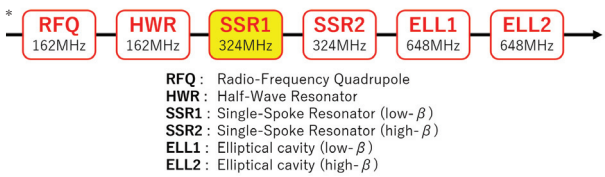

Figure 1: Accelerating structure proposed for the JAEA-ADS linac.

As the first step toward the full-scale design of the JAEA-ADS linac, we are planning to demonstrate a high-field cavity test by prototyping a low-beta single-spoke resonator (SSR1). A single-spoke cavity is one of the 2-cell $\lambda/2$-structure cavities. This prototyping will provide us various insights about developing SC $\lambda/2$ resonant cavities. Moreover, through the high-field cavity test, we will acquire valuable information such as how much accelerating gradient would be achievable with the required stability. In this paper, the present status of the spoke cavity prototyping is presented.

DESIGNED PROTOTYPE SPOKE CAVITY

We investigated the electromagnetic design of the prototype spoke cavity which operating frequency (f_0) is 324 MHz. The unit cell length defined as the distance between the two gap centers was fixed to $\beta_g\lambda/2 = 87.0$ mm, where β_g and λ represent the geometrical beta and the resonant wavelength, respectively. The dimensional parameters of the design model were optimized for higher cavity performance [3]. Figure 2 shows the electric (left) and magnetic (right) distributions of the designed cavity. The accelerating field distribution along the beam axis is shown in Fig. 3. The transit time factor as a function of beam velocity (β) obtained by

$$T(\beta) = \frac{\int E_z(z)\sin\left(\frac{2\pi}{\beta\lambda}z\right)dz}{\int |E_z(z)|dz} \quad (1)$$

is shown in Fig. 4. One can see that the transit time factor is maximized with the beam velocity of $\beta = 0.24$ (optimal beta : β_{opt}). Assuming that the beam velocity is at the optimal

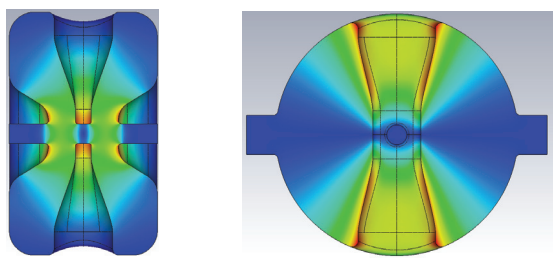

Figure 2: Electric field distribution on Y-Z plane (left) and magnetic field distribution on X-Y plane (right).

* jtamura@post.j-parc.jp

ISBN: 978-3-95450-233-2 ISSN: 2673-5504 doi:10.18429/JACoW-SRF2021-WEPCAV011

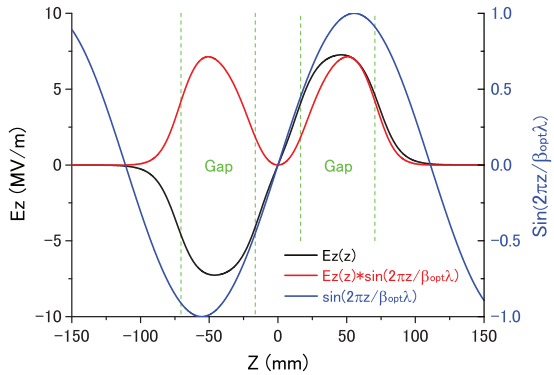

Figure 3: Accelerating field distribution along the beam axis. The field strength is normalized to have the stored energy of 1 Joule.

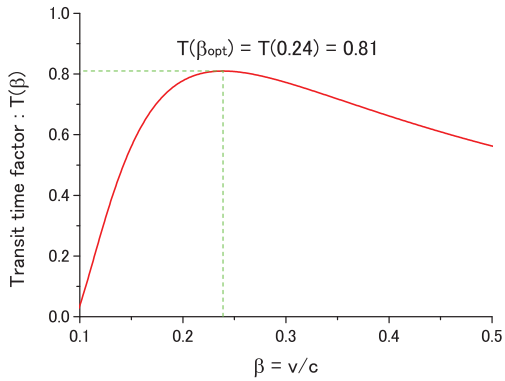

Figure 4: Transit time factor as a function of beam velocity obtained by the electric field distribution along the beam axis.

beta ($\beta = \beta_{\rm opt}$), the accelerating voltage is defined as

$$V_{\rm acc} = V_0 T(\beta_{\rm opt}) = \int E_z(z) \sin\left(\frac{2\pi}{\beta_{\rm opt}\lambda} z\right) dz \qquad (2)$$

where V_0 is an axial RF voltage : $V_0 \equiv \int |E_z(z)| dz$. By defining the effective length as $L_{\rm eff} = \beta_{\rm opt}\lambda$ [4], the accelerating gradient is obtained as $E_{\rm acc} = V_{\rm acc}/L_{\rm eff}$. The design parameters of the prototype spoke cavity is listed in Table 1. The figures of merit are comparable with that of a modern single spoke cavity [5]. The multipactor analysis for the prototype spoke cavity without coupler ports was also performed [6].

COUPLER PORT

Two dedicated ports for RF couplers are introduced to the cavity's side shells. The axis direction of the coupler ports is orthogonal to the spoke electrode as shown in Fig. 5. In order to sufficiently high-pressure rinse (HPR) all the inner surface of the cavity with ultrapure water, the water

Table 1: Design Parameters of the Prototype Spoke Cavity

Parameter	Value
f_0	324 MHz
$\beta_{\rm g}$	0.188
$\beta_{\rm opt}$	0.24
Beam aperture	40 mm
Cavity diameter	$\approx$ 500 mm
Cavity length	300 mm
$L_{\rm eff} = \beta_{\rm opt}\lambda$	222 mm
$G = Q_0 R_{\rm s}$	90 Ω
$T(\beta_{\rm opt}) = V_{\rm acc}/V_0$	0.81
$R_{\rm sh}/Q_0 = V_{\rm acc}^2/\omega W$	240 Ω
$E_{\rm peak}/E_{\rm acc}$	4.1
$B_{\rm peak}/E_{\rm acc}$	7.1 mT/(MV/m)

spray nozzle needs to be inserted into the cavity through the coupler ports and the beam ports. If we focus only on the effectiveness of the HPR, a shorter port length is preferable because the watering nozzle can go inside the cavity with a wider angle and can spray ultrapure water into a larger area of the cavity's inner surface.

As a result of the investigation on the suitable coupler-port length, we determined the port length as 60 mm. Contrary to the demand arising from the effective HPR mentioned above, the port length should be long enough not to affect the superconducting state of the cavity even when the port-end faces are covered by NC materials. The RF losses dissipated in each surface ($P_{\rm port}$ in the end faces of the coupler ports, $P_{\rm cav}$ in the cavity except the end faces of the coupler ports, and $P_{\rm total} = P_{\rm cav} + P_{\rm port}$) were evaluated by corresponding Q-values defined by,

$$Q_{\rm port} = \frac{\omega W}{P_{\rm port}} \qquad (3)$$

$$Q_{\rm cav} = \frac{\omega W}{P_{\rm cav}} \qquad (4)$$

$$Q_{\rm total} = \frac{\omega W}{P_{\rm total}} = \frac{\omega W}{P_{\rm cav} + P_{\rm port}} \qquad (5)$$

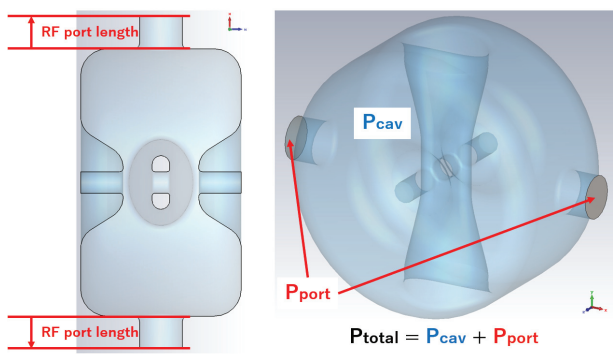

Figure 5: Configuration of the coupler ports. The inner diameter of the coupler ports is ϕ80 mm.

ISBN: 978-3-95450-233-2 ISSN: 2673-5504 doi:10.18429/JACoW-SRF2021-WEPCAV011

Table 2: Q-values Obtained by the Simulation with the Coupler Port Length of 60 mm

Temperature conditions	Q_{cav}	Q_{port}	Q_{total}
Cav @ 4.2K (R_s = 51 nΩ), Port @ 4.2K (R_s = 51 nΩ)	1.76×10^9	2.63×10^{17}	1.76×10^9
Cav @ 4.2K (R_s = 51 nΩ), Port @ NC ($\sigma = 1.35 \times 10^6$ S/m)	1.76×10^9	4.35×10^{11}	1.76×10^9
Cav @ 2.0K (R_s = 11 nΩ), Port @ 2.0K (R_s = 11 nΩ)	8.12×10^9	1.21×10^{18}	8.12×10^9
Cav @ 2.0K (R_s = 11 nΩ), Port @ NC ($\sigma = 1.35 \times 10^6$ S/m)	8.12×10^9	4.35×10^{11}	7.97×10^9

where ω and W represent the angular frequency and the stored energy, respectively. Each Q-value obtained by the post-processing of the eigenmode solver of CST Microwave Studio (CST MWS) are listed in Table 2. Here, the surface resistance under SC condition were chosen as R_s = 51 nΩ for 4.2 K and R_s = 11 nΩ for 2.0 K. Regarding the surface resistance of the NC material, the electric conductivity in the end faces of the coupler port was set as $\sigma = 1.35 \times 10^6$ S/m assuming a stainless-steel flange. Therefore, the NC surface resistance is derived as $R_s = 3.1 \times 10^{-2}$ Ω by $R_s = \sqrt{\omega\mu/2\sigma}$ where μ is the magnetic permeability. According to the estimated Q-values in each surface listed in Tab. 2, the RF loss dissipated in the coupler port ends is sufficiently lower than that in the cavity.

INPUT POWER COUPLER

The antenna position of the input power coupler which would realize the critical-coupling condition was examined. Figure 6 shows the antenna configuration (left) and the external Q-value (Q_{ext}) dependence on the antenna position (right). In the vertical cavity testing where no beam is accelerated, the optimal antenna position determined by

$$Q_{ext} = Q_0 \tag{6}$$

would be 68 mm outside the cavity assuming the unloaded Q-value as $Q_0 \sim 1 \times 10^9$. When beam loading (P_{beam}) exists, the optimal antenna position would be determined by

$$Q_{ext} \sim \frac{V_{acc}^2}{P_{beam} \cdot (R_{sh}/Q_0)} \tag{7}$$

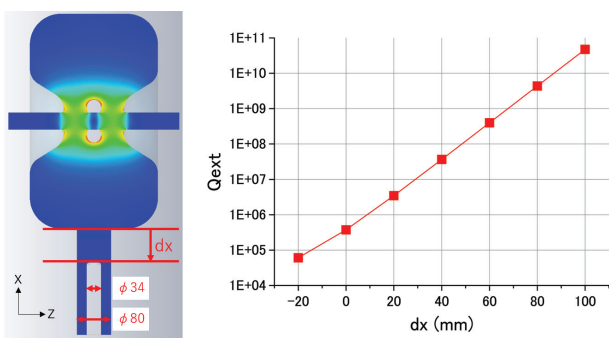

Figure 6: [Left] Configuration of the input coupler antenna. [Right] Q_{ext} with respect to the antenna position obtained by the eigenmode solver of CST-MWS.

Therefore, if we assume V_{acc} = 1.6 MV/m and P_{beam} = 30 kW just as a possible example, the desired Q_{ext} would be 3.6×10^5 with the antenna position at $dx \sim 0$.

CAVITY PARTS MANUFACTURING

In order to proceed to an actual cavity prototyping, we have reviewed the fabrication process. Figure 7 shows the cavity disassembly. During the cavity fabrication, the resonant frequency will be tuned to the targeted value by adjusting the longitudinal cavity length. By this adjustment, the two gap-length will be shortened, and this will lead to the frequency decrease.

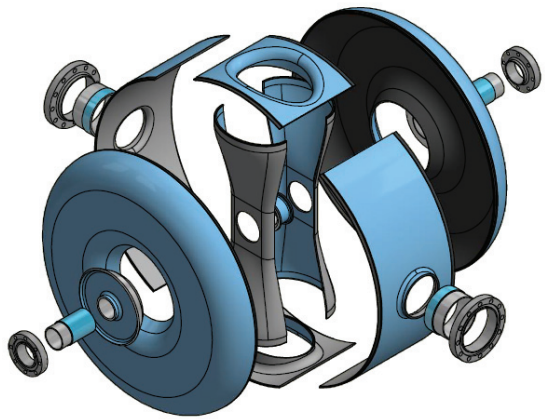

Figure 7: Prototype spoke cavity divided into each part.

We examined the electron-beam welding (EBW) using niobium test pieces and investigated the welding condition for realizing the smooth underbead. One example of the test result is shown in Fig. 8. We expect further investigation on the welding condition before the actual cavity fabrication.

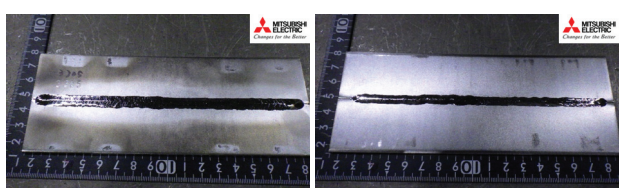

Figure 8: Example of the plain butt-welding result. [Left] Front side of the niobium test pieces. [Right] Reverse side of the niobium test pieces.

ISBN: 978-3-95450-233-2 ISSN: 2673-5504 doi:10.18429/JACoW-SRF2021-WEPCAV011

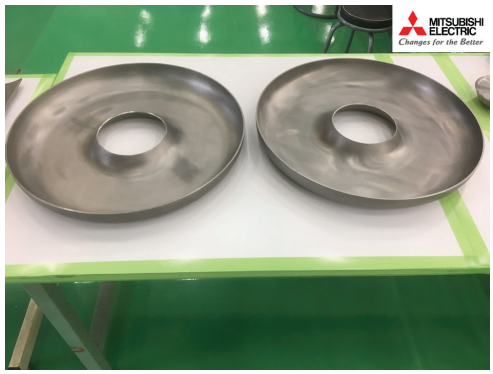

Figure 9: End plates (Lids).

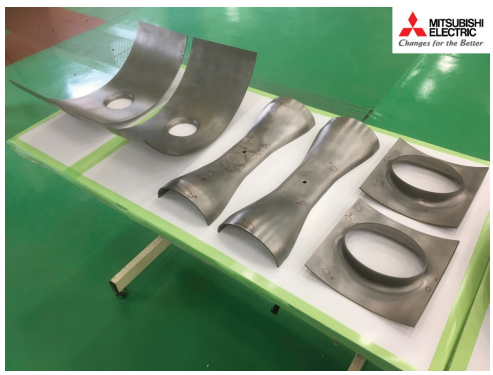

Figure 10: From left to right: side shells, spoke electrodes, and spoke roots.

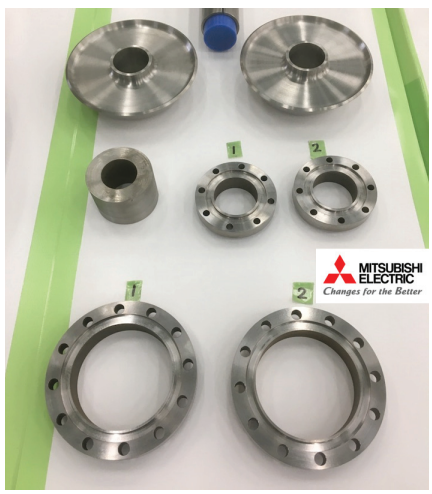

Figure 11: Drift tubes and port flanges.

We have eventually started the press forming of niobium sheets (t3.5 mm) and the machine work to shape the cavity parts. The press-forming test using aluminum sheets with the same thickness preceded the actual niobium pressing work. Figures 9 and 10 show the niobium cavity parts shaped by the press work. The side shells and the spoke roots were press-formed after being shaped by bending work. The drift tubes (one drift tube in the spoke electrode and two nose-shaped drift tubes in the end plates) were machined from pure niobium brocks. The port flanges (two for the beam ports and two for the RF coupler ports) were machined from niobium-titanium alloy. Figure 11 shows the drift tubes and the port flanges.

SUMMARY

We have finally started prototyping the low beta spoke cavity (SSR1) for the JAEA-ADS linac. Before the actual cavity fabrication, the fabrication process was carefully reviewed. After the various examinations such as the EBW test using niobium test pieces and the press-forming test using alminum sheets, we proceeded to manufacture the niobium cavity parts. Now, we are preparing for the electron-beam welding of the shaped cavity parts.

ACKNOWLEDGMENT

We would like to thank the staff of Mitsubishi Electric, Ltd. for prototyping the spoke cavity.

REFERENCES

[1] B. Mustapha, S. V. Kutsaev, J. A. Nolen, and P. N. Ostroumov, "A compact linac design for an accelerator driven system", in *Proc. 27th Linear Accelerator Conf. (LINAC'14)*, Geneva, Switzerland, Aug.-Sep. 2014, paper MOPP003, pp. 52–54.

[2] B. Yee-Rendon, Y. Kondo, J. Tamura, S. Meigo, and F. Maekawa, "Progress on SRF linac development for the accelerator-driven subcritical system at JAEA", presented at SRF'21, East Lansing, MI, USA, Jun. 2021, paper TUP-FAV001, this conference.

[3] J. Tamura *et al.*, "Electromagnetic design of the Prototype Spoke Cavity for the JAEA-ADS Linac", in *Proc. 19th Int. Conf. RF Superconductivity (SRF'19)*, Dresden, Germany, Jun.-Jul. 2019, pp. 399–402. doi:10.18429/JACoW-SRF2019-TUP007

[4] A. Facco, "Tutorial on low beta cavity design", in *Proc. 12th Int. Conf. RF Superconductivity (SRF'05)*, Ithaca, NY, USA, Jul. 2005, paper SUA04, pp. 21–33.

[5] M.H. Awida *et al.*, "Development of low β single-spoke resonators for the front end of the Proton Improvement Plan-II at Fermilab", *IEEE Trans. Nucl. Sci.*, vol. 64, no. 9, Sept. 2017. doi:10.1109/TNS.2017.2737560

[6] J. Tamura *et al.*, "RF design of the Prototype Spoke Cavity for the JAEA-ADS linac", in *Proc. 3rd J-PARC Symposium (J-PARC2019)*, Tsukuba, Japan, Sept. 2019, p. 011049. doi:10.7566/JPSCP.33.011049